SUPPLEMENTARY INFORMATION

The Structure of the Integrin αIIbβ3 Transmembrane Complex Explains Integrin Transmembrane Signaling

Tong-Lay Lau[1], Chungho Kim[2], Mark H. Ginsberg[2] and Tobias S. Ulmer[1]

[1]Department of Biochemistry & Molecular Biology and Zilkha Neurogenetic Institute, Keck School of Medicine, University of Southern California, 1501 San Pablo Street, Los Angeles, CA 90033

[2]Department of Medicine, University of California San Diego, 9500 Gilman Drive, La Jolla, CA 92093

TABLE OF CONTENTS

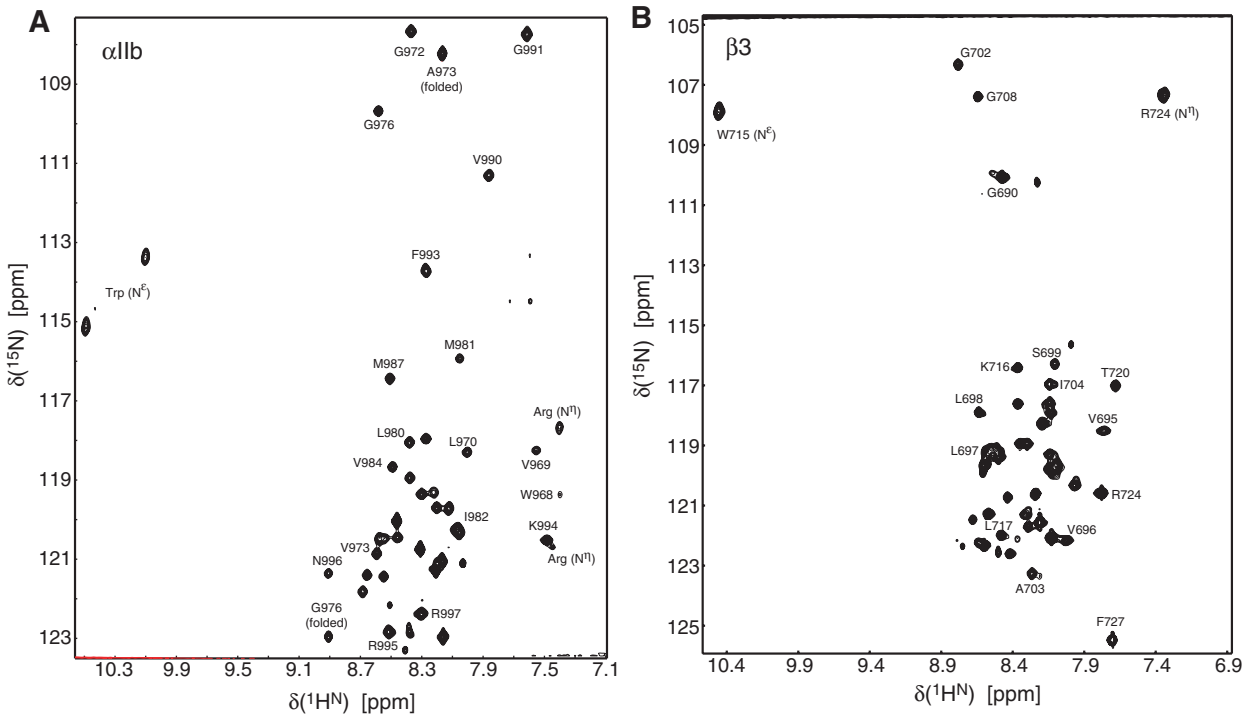

Supplementary Figure 1. H-N correlation spectra of free, monomeric αIIb and β3 TM segments. Well-resolved H-N resonances are labeled. Note that monomeric and heterodimeric αIIb spectra were recorded with slightly different ^{15}N spectral width to optimize data acquisition. Samples were prepared using bicelles composed of 385 mM 1,2-Dihexanoyl-*sn*-Glycero-3-Phosphocholine, 83 mM 1-Palmitoyl-2-Oleoyl-*sn*-Glycero-3-Phosphocholine, 41 mM 1-Palmitoyl-2-Oleoyl-*sn*-Glycero-3-[Phospho-L-Serine].

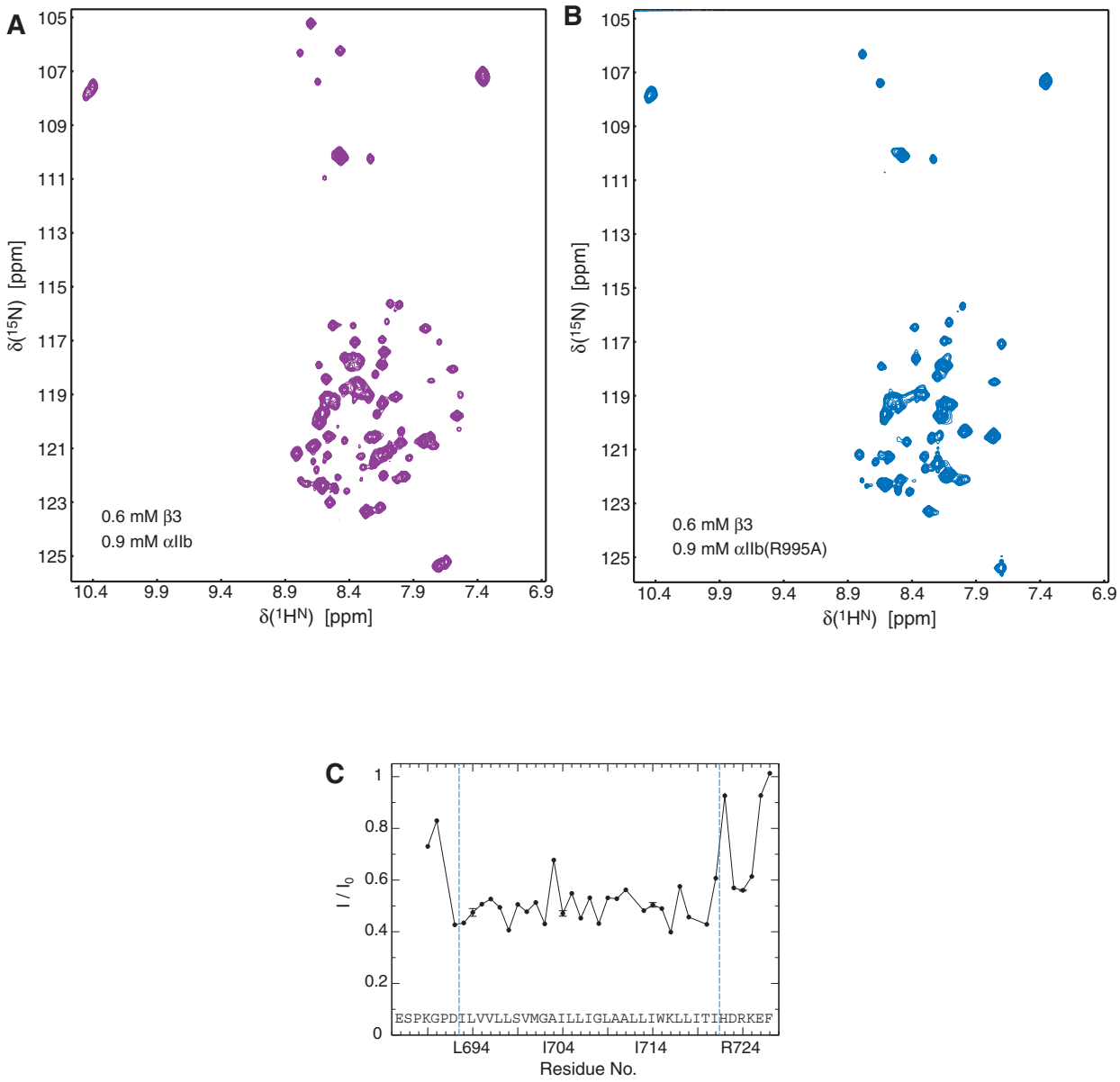

Supplementary Figure 2. Effect of αIIb(R995A) peptide upon heterodimerization. (**A-B**) Upon introducing the αIIb(R995A) substitution, the heterodimeric β3 backbone H-N resonances are either lost or greatly diminished compared to wild-type αIIb at identical experimental conditions (385 mM 1,2-Dihexanoyl-*sn*-Glycero-3-Phosphocholine, 83 mM 1-Palmitoyl-2-Oleoyl-*sn*-Glycero-3-Phosphocholine, 41 mM 1-Palmitoyl-2-Oleoyl-*sn*-Glycero-3-[Phospho-L-Serine].). (**C**) However, the resonance intensities at their monomeric positions (Supplementary Figure 1B) are still affected by the presence of αIIb(R995A) as depicted by the signal intensity ratios, I/I_0, of β3 in the presence and absence of αIIb(R995A), respectively. This indicates the presence of additional heterodimerization elements and, on the timescale of the NMR measurements, reflects a transition from the slow to the fast exchange limit. In other words, the αIIb(R995A) weakens heterodimerization, but does not abrogate it completely in agreement with additional αIIb-β3 heterodimerization elements (see Figure 5).

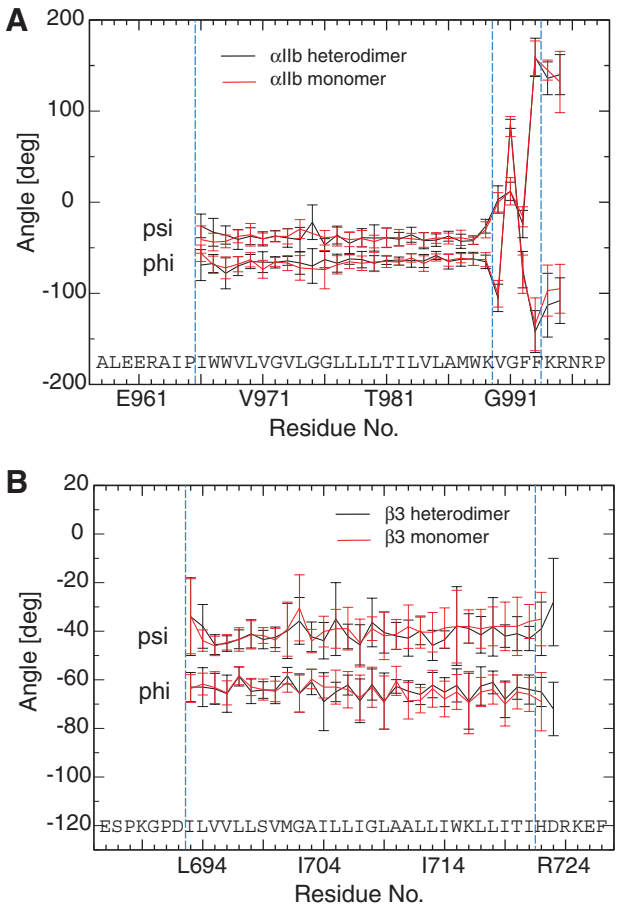

Supplementary Figure 3. Comparison of chemical shift-based backbone torsion angle predictions between monomeric and heterodimeric states. TALOS-based predictions using H^{α}, N, C^{α} and C′ chemical shifts. Monomeric and heterodimeric backbone conformations are identical within prediction uncertainties.

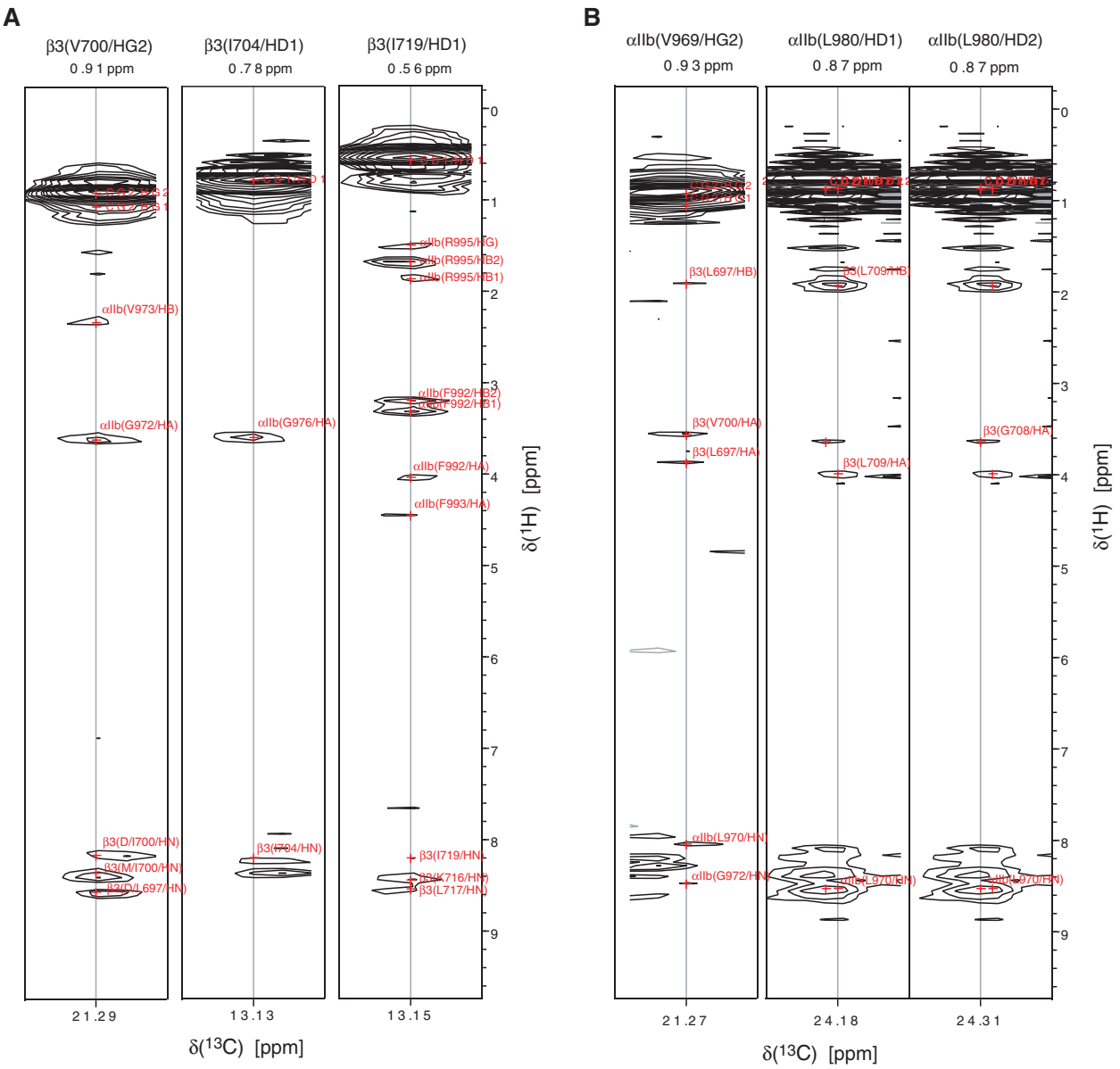

Supplementary Figure 4. Illustration of αIIb-β3 intersubunit NOEs. Representative strip plots of, (**A**), selectively Val-$\gamma^{1,2}$ ($^{13}CH_3/^{12}CD_3$), Leu-$\delta^{1,2}$ ($^{13}CH_3/^{12}CD_3$), Ile-δ^1 ($^{13}CH_3$)-labeled β3 in combination with fully protonated αIIb and, (**B**), selectively Val-$\gamma^{1,2}$ ($^{13}CH_3/^{12}CD_3$), Leu-$\delta^{1,2}$ ($^{13}CH_3/^{12}CD_3$), Ile-δ^1 ($^{13}CH_3$)-labeled αIIb in combination with fully protonated β3. Intersubunit NOEs are indicated. Intersubunit methyl-methyl NOEs could not be identified due to the dominance of the intrasubunit methyl signal. Intersubunit methyl to H^{α}, H^{β} and H^{γ} NOEs were readily identifiable, as indicated. NOEs between methyl groups and back-exchanged H^N nuclei are also marked. NOE mixing times and exchange kinetics (temperature) were extensively screened to optimize the relatively weak transferred NOE amplitudes (fast exchange limit) and the ratio of associated to dissociated states (slow exchange limit) in the non-covalently associated complex.

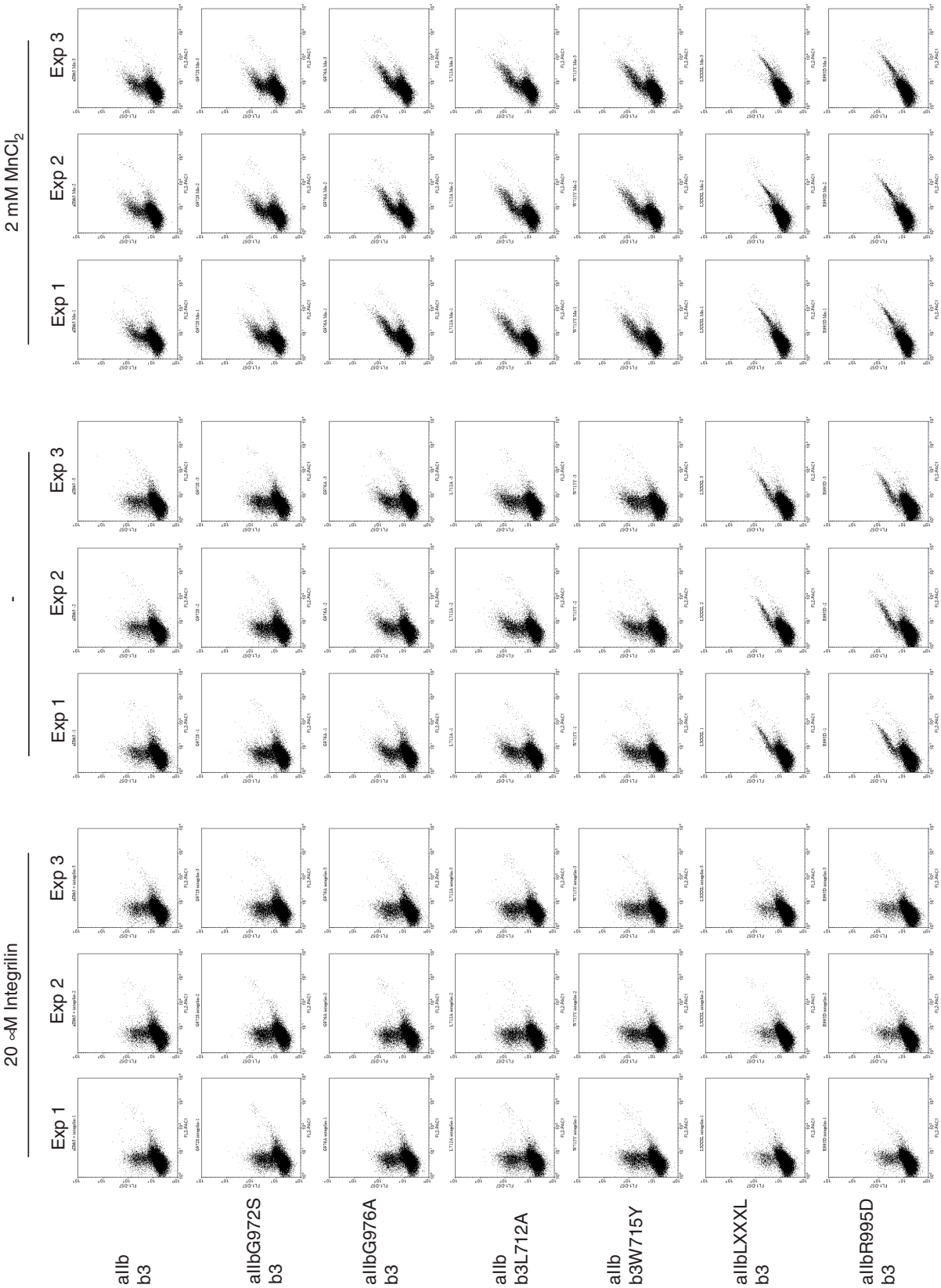

Supplementary Figure 5. Flow cytometric activation assays of selected point mutations (c.f. Figure 8).

Supplementary Table I. Compatibility of heterodimeric backbone torsion angle restraints and H^N-H^N NOEs with monomeric αIIb and β3 transmembrane structures[a]

R.m.s. deviations from experimental dihedral (ϕ/ψ) restraints (deg)	
All *(121)*	1.03 [b]
R.m.s. deviations from experimental distance (H^N-H^N) restraints (Å)	
All (*100*)	0.08
Interresidue sequential (|i – j| =1) (*50*)	0.06 [c]
Interresidue short range (1 < | i – j| < 5) (*50*)	0.11 [c]

a, PDB ID 2k1a and 2mrz, average structures

b, The r.m.s.d. upon refining directly against these restraints is comparable (see Supplementary Table II).

c, The r.m.s.d. upon refining directly against these restraints is only marginally lower (see Supplementary Table II).

Supplementary Table II. Structural statistics for the αIIb-β3 transmembrane complex[a]

R.m.s. deviations from experimental dihedral restraints (deg)	
All *(145)*[b]	1.28 ± 0.14
R.m.s. deviations from experimental distance restraints (Å)	
All (*127*)	0.04 ± 0.01
Interresidue sequential (|i – j| =1) (*50*)	0.01 ± 0.01
Interresidue short range (1 < | i – j| < 5) (*50*)	0.05 ± 0.01
Interresidue long range (|i – j| ≥ 5) (*27*)	0.06 ± 0.02
Deviations from idealized covalent geometry	
Bonds (Å)	0.003 ± 0.000
Angles (deg)	0.495 ± 0.018
Impropers (deg)	0.326 ± 0.020
Coordinate precision (Å)[c]	
Backbone non-hydrogen atoms	0.68
All non-hydrogen atoms	1.05
Measures of structural quality	
E_{LJ} (kcal·mol^{-1})^3 [d]	-295.9
Residues in most favorable region of Ramachandran plot [e]	100%

a, Statistics for the 20 calculated simulated annealing structures, encompassing residues αIIb(I966-R995) and β3(I693-D723).

b, Torsion angles included 121 ϕ/ψ and 24 χ_{1-4} angle restraints. χ_{1-4} restraints set snorkeling/rotamer preferences.

c, Defined as the average r.m.s. difference between the final 20 simulated annealing structures and the mean coordinates.

d, The Lennard–Jones van der Waals energy was calculated with the CHARMM PARAM 19/20 parameters and was not included in the simulated annealing target function.

e, PROCHECK V3.4.4 (Roman A. Laskowski, Malcolm W. MacArthur, David S. Moss and Janet M. Thornton (1993). PROCHECK: a program to check the stereochemical quality of protein structures. J. Appl. Cryst., 26, 283-291)